Journal of Structural Geology 31 (2009) 260–269

Contents lists available at ScienceDirect

Journal of Structural Geology

journal homepage: www.elsevier.com/locate/jsg

Geometric and kinematic modeling of detachment folds with growth strata based on Bézier curves☆

Chun Liu*, Yikun Zhang, Bin Shi

School of Earth Sciences and Engineering, Nanjing University, 22 Hankou Road, Nanjing 210093, Jiangsu, China

ARTICLE INFO

Article history:
Received 10 May 2008
Received in revised form
9 November 2008
Accepted 26 November 2008
Available online 16 December 2008

Keywords:
Detachment folds
Bézier curve
Geometric model
Kinematic model
Growth strata

ABSTRACT

In our geometric modeling, the inner layer of competent rock units in a detachment fold is approximated by several quadratic Bézier curves, which are joined together according to some geometrical rules, whereas the outer layers are calculated from the inner layer by parallel folding mechanism. In this model, an ideal fold is determined by three parameters: w, half of the distance between the locations of the fold's two limbs where their dips are measured, θ_1 and θ_2, the dip angles of its two limbs. Two more parameters, respectively the axial lift-up ratio (u) and the limb elongation (E) may be used to change the ideal fold shape, if necessary. In kinematic modeling, downward deflection in the two synclines flanking an anticline is assumed to maintain constant area during folding. Both mathematical derivation and numerical simulation show that the reduction of the balanced area (A_r) is directly proportional to the downward deflection angle (φ), and there is an approximate linear relationship between the detachment depth and the downward deflection angle. Based on this relationship, an iterative method is used to find the approximate value of φ. Furthermore, syn-folding growth strata can be modeled through calculating the velocity field above a detachment fold during folding. The method is applied to three seismic interpretation cross-sections of detachment folds respectively in Tarim Basin (western China), Zagros fold-belt (Iran) and Niger delta (western Africa). Variations of φ with the development of the detachment folds indicate the transfer of rock materials between the synclinal and anticlinal areas of the folds.

1. Introduction

Detachment folds are defined by competent rock units and are cored by incompetent rock units that are deformed internally above the detachment horizon. They represent a major structural type of fold- belts and control the localization of some important mineral resources such as oil and gas (Scharer et al., 2004; Gonzalez-Mieres and Suppe, 2006). Precise geometric description and kinematic simulation of detachment folds provide important clues with the origin and evolution of these structures.

Previous studies have dealt with the geometric and kinematic models of detachment folds. Homza and Wallace (1995) regarded a detachment fold as a triangle, and presented a fixed and variable detachment depth model. Bulnes and Poblet (1999) evaluated four different methods for estimating detachment depth beneath detachment folds, and presented a new, simple method, using information from more than one stratigraphic horizon. By joining several triangles and quadrangles to describe a fold, Mitra (2003) developed a kinematic model of detachment folds with growth of the synclines on the sides of two limbs of an anticline. Wilkerson et al. (2007) illustrated the utility of some previous models by constructing pseudo three -dimensional representations of natural folds, and presented two new two-dimensional geometric and kinematic models for detachment folds that respectively incorporate hinge migration and limb rotation as their deformation mechanisms.

In these geometric models, fold layers are usually approached by a series of line segments. No doubt, connection of line segments merely gives a rough approximation to a fold shape, while curves can describe the change of a fold shape more precisely. Numerous previous studies concerned with the curved fold shape, in which a fold is approached by a series of special curves that are defined by some mathematical functions. Stabler (1968) and Chapple (1969) have used the Fourier analysis in quantitative description of fold shapes. Hudleston (1973) improved the method, using only two Fourier coefficients to classify the shape of folds. However, his method only gives a rough approximation of the functions of fold shapes. Twiss (1988) has studied the geometrical properties of folds

☆ Information and software for the fold simulation developed in this paper are available online: http://www.acei.cn/program/folds.htm.

* Corresponding author. Tel.: +86 25 8368 6797; fax: +86 25 8359 6220.
E-mail addresses: oxtown@gmail.com, oxtown@hotmail.com (C. Liu).

0191-8141/$ – see front matter © 2008 Elsevier Ltd. All rights reserved.
doi:10.1016/j.jsg.2008.11.019

and has proposed a description method of symmetric folded surfaces by three fold style parameters. Bastida et al. (1999) proposed a method to approach fold shapes with the power functions. Their method of describing a fold is based on two parameters: the exponent, n, describing the shape, and the amplitude-wavelength ratio. Srivastava and Lisle (2004) used computer-aided Bézier curve analysis and reduced eight variables of a cubic Bézier curve to two variables for describing a fold. However, these methods are mainly used in fold description and classification. When they are applied to geometric and kinematic simulation of a fold, many difficult problems appear. For example, several segments of curves should be joined in order to approach fold shape, since it is hard to describe a fold by only one curve. The crux of the problem is to find the relationship between these curve segments, by which the curves can be joined smoothly and show a reasonable change in the evolution of the structure.

In this paper, we present a new geometric model of detachment folds based on quadratic Bézier curves and provide a possible new way for classification of folds. We do not assume that the model represents all natural detachment folds. Rather, a natural detachment fold may be approximated by varying several parameters. Based on the geometric model, a kinematically balanced model of detachment folds and growth strata is also presented. The new model proposed in this paper is designed for computer implement.

2. Geometric model

Bézier curves are a basic and important tool of computer graphics, which is firstly used in the automobile industry to describe curvatures and surfaces (Bézier, 1966, 1967). Recently, the method has been introduced into geological literature (De Paor, 1996) and was used as a tool for fold shape analysis (Srivastava and Lisle, 2004) and flanking structure description (Coelho et al., 2005). Since then, the Bézier curves have demonstrated their versatility for analyzing a wide range of fold geometries. However, in previous studies (Srivastava and Lisle, 2004; Coelho et al., 2005), the Bézier curves were mainly used in classification and fold shape analysis, not for kinematic simulation. In our method, it is supposed that the curve can be uniquely determined by three points (one hinge point and two deflection points) and two tangents which represent the dips of two fold limbs. Based on this, we have chosen the quadratic Bézier curves.

2.1. Quadratic Bézier curves

Generally, a quadratic Bézier curve is uniquely determined by the position of three points (Fig. 1): two points, $P_0(x_0, y_0)$ and $P_2(x_2, y_2)$, are at the two ends of the curve and one further control point, $P_1(x_1, y_1)$, between them. The parametric equations of a quadratic Bézier curve are (Bézier, 1966, 1967; Sun and Hu, 2005):

$$\begin{aligned} x(t) &= (1-t)^2 x_0 + 2(1-t)t x_1 + t^2 x_2 \\ y(t) &= (1-t)^2 y_0 + 2(1-t)t y_1 + t^2 y_2 \end{aligned} \quad (1)$$

The parameter t indicates the position along the Bézier curve from the start point P_0, where $t = 0$, towards the end point P_2, where $t = 1$. The quadratic Bézier curve, made up of a succession of points corresponding to different t values, is consequently defined by the coordinates of points P_0, P_1 and P_2.

Start points and end points are usually defined as the inflection points or hinge points of folded layer (Srivastava and Lisle, 2004). Control point P_1 that has no geological equivalent should be determined by some other geometric elements of structures, such as angles and spans, which can be directly measured from field examples (Coelho et al., 2005). Since P_0P_1 and P_2P_1 are the tangent

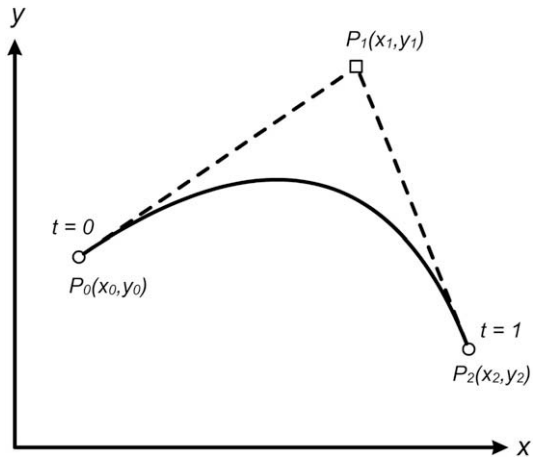

Fig. 1. A quadratic Bézier curve can be defined by three control points: P_0, P_1, P_2. Since P_0P_1 and P_2P_1 are the tangents at the points P_0 and P_2, respectively, the curve can be redefined by P_0, P_2 and the slope of corresponding tangents.

at the points P_0 and P_2 respectively, the quadratic Bézier curve can also be determined by the two end points (P_0, P_2) and the slope (k_0, k_2) of the corresponding line segments (P_0P_1 and P_2P_1). The two parameters, x_1 and y_1 in Eq. (1) can be replaced by the slopes:

$$\begin{aligned} x_1 &= (k_0x_0 - k_2x_2 + y_2 - y_0)/(k_0 - k_2) \\ y_2 &= (k_0k_2x_0 - k_0k_2x_2 - k_2y_0 + k_0y_2)/(k_0 - k_2) \end{aligned} \quad (2)$$

2.2. Ideal detachment fold

In this section, an ideal fold with rounded shape and constant orthogonal thickness is drawn by a simple geometric procedure based on the new geometric model of folds. In this method, a fold is divided into three parts by its two inflection points (the points H and I in Fig. 2c); and each part is approximated by two Bézier curves, which are connected at their hinge point (the point K in Fig. 2c). Therefore, inner layer of the fold is composed of six Bézier curves.

An ideal fold can be drawn by five steps:

(1) Confine the area of the fold. Draw an isosceles triangle ABC, in which the points B and C represent the inflection points on the fold limbs. AB and AC are the corresponding tangents of the folded surface at the inflection points. The angles that AB and AC form with the x axis represent the limb dips (θ_1 and θ_2). The origin of the coordinates is set at point O with AO being the bisector line of $\angle BAC$. Hence, $BO = CO = w$, where w is a parameter that can be used to describe the size of the fold.
(2) Find the core of the fold. Draw BD and CE perpendicular to AB and AC, respectively, and let $BD = CE = w$. Then, draw perpendiculars to BD and CE from D and E, respectively. The two perpendiculars intersect at the point F, which is defined as the fold core. Find another point G along the direction of FA, which makes $FG = w$. The point G and the line segment FG are defined as the hinge point and the fold axial plane, respectively. Note that since the triangle ABC is an isosceles triangle, F and G should be on the line AO (Fig. 2b).
(3) Draw the center part. Mark the end points of each bed on segments BD, FG and CE equidistantly. The points, H, K and I, are the end points of the bottom layer of competent rock units. Connect the corresponding end points with two Bézier curves, one Bézier curve with the end points H and K and the other K and I. Each of the two Bézier curves is drawn according to the

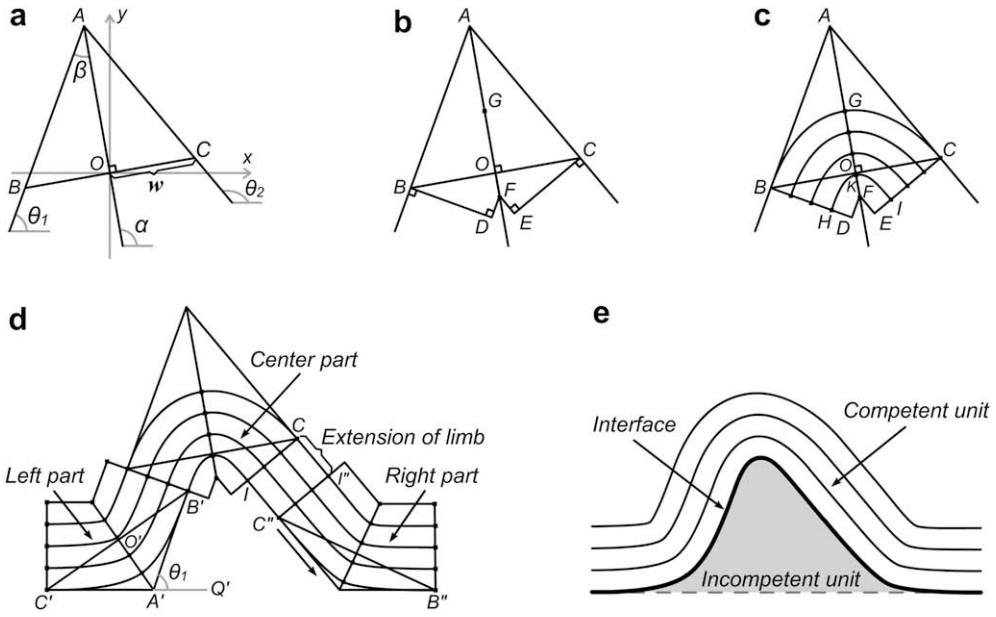

Fig. 2. The geometric modeling of an ideal detachment fold. (a) Draw an isosceles triangle *ABC*, in which the angles that segment *AB* and *AC* form with the *x* axis are θ_1 and θ_2 (limb dips), respectively. (b) Find the fold core *F* and the hinge point *G*, which make $FG = BD = CE$. (c) The end points of each bed on segments *BD*, *FG* and *CE* are marked equidistantly, by which two curves are illustrated to compose the inner layer. Afterward, the outer layers of competent rock units are calculated from the inner layer by parallel folding mechanisms. (d) Two limbs can be drawn according to the similar rules as the center part. (e) Finally, the ideal detachment fold is obtained.

position of its two end points and the slope at the end points in Eqs. (1) and (2). The common slope of the two Bézier curves at the hinge point *K*, where they are connected, is assumed to be perpendicular to the fold axial plane while the slopes at the end points *H* and *I* are given as the dips of fold limbs (θ_1 and θ_2 respectively). The overlying layers of competent rock units in the fold are drawn layer by layer upward according to the bottom layer based on the principle of iso-thickness. The center part of the fold (Fig. 2c) is determined by *w*, θ_1 and θ_2.

(4) Draw the left part. The left side of the left part of the fold should be connected with the horizontal strata, while the other side with the beds of the center part of the fold along the line segment *BD*. Just repeat the steps (1)–(3) to draw the left part (Fig. 2d).

(5) Draw the right part. Since the slope of the right limb is smaller than the slope of the left limb in this demonstration, the right limb should be extended along the direction of *C* to *I*″ in order to maintain the strata at the two ends of the fold to be on the same level (Fig. 2d).

Eventually, the ideal detachment fold geometry (Fig. 2e) is determined by three parameters: *w*, θ_1 and θ_2.

2.3. Axial lift-up ratio and limb elongation

There is an approximate uniform curvature distribution between the hinge point and the inflection point of an ideal detachment fold. In order to simulate more types of folds, such as chevron folds with straight limbs and curvature concentrated at the hinge and box folds with curvature concentrated in two corners. A new parameter *u*, which means axial lift-up ratio, is defined to determine the curvature distribution of folded layers:

$$u = l_{KL}/l_{JL} \tag{3}$$

where l_{KL} and l_{JL} represent the length of line segments KL and JL in Fig. 3, in which *H*, *K* and *I* are the three control points of the bottom layer of competent rock units (see also Fig. 2c); the point *J* is determined from the inflection points *H* and *I* and the dips of two fold limbs (*JH* and *JI* are parallel to *AB* and *AC*, respectively).

Fig. 3 shows how the parameter *u* controls the distribution of curvature in a fold. One end of the fold shape spectrum, $u = 0$, approximately corresponds to box folds, while the other end, $u = 1$, corresponds to chevron folds. When $0 < u < 1$, the fold shape spectrum shows a gradual change between the above two end types of folds.

In the fifth step of modeling an ideal detachment fold, the right limb is extended in order to maintain the horizontal strata of two fold limbs on the same level (Fig. 2d). A parameter *E* is used to represent the limb elongation, which is defined to be:

$$E = l_{CI''}/w \tag{4}$$

where $l_{CI''}$ represents the length of line segment *CI*″ in Fig. 2d; and *w* is the parameter, mentioned above, used to describe the size of the fold.

Eventually, the shape of a detachment fold can be determined by the following parameters: θ_1, θ_2, u_l, u_c, u_r, E_l and E_r, where the subscripts l, c and r represent the parameters of the left part, center part and right part, respectively. For example, u_c means the axial lift-up ratio of the center part.

3. Kinematic model

A balanced kinematic model of detachment folds is presented in this section, which is based on the geometric model described in the previous section. In order to simulate the development of a detachment fold, we will make two kinematic assumptions: (1) the fold initiates, or rapidly develops, with a high wavelength-amplitude ratio, with the fold wavelength determined by the thickness of the competent unit (Biot, 1961; Currie et al., 1962). (2) The two limbs (or synclinal areas) are deflected below their regional position in the evolution (Mitra, 2003), to maintain area balanced and to be kinematically admissible.

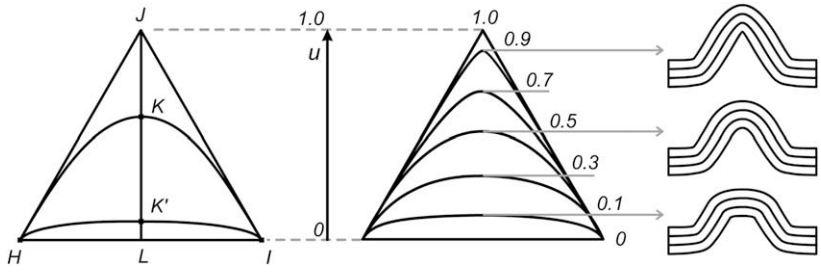

Fig. 3. Axial lift-up ratio: $u = l_{KL}/l_{JL}$. The folded surface changes from box form to chevron form when u increases from 0 to 1.0.

According to the first assumption, the initial conditions of a detachment fold are assumed as: $\theta_1 = 0°$, $\theta_2 = 180°$. Then, if the final conditions and the deformation mechanism are given, a series of intermediate states of the fold could be computed and drawn by the program (see the article footnote for additional information of the program).

The second assumption is determined by the first one. If a detachment fold initiates with a high wavelength-amplitude ratio, the excess area of the fold above the regional datum (A_1) is too high compared to the shortened area (A_2) (Fig. 4a; see also Fig. 9a, Mitra, 2003). This problem can be solved, taking a downward deflection of the two limbs (i.e., forming two synclinal areas) below the regional datum into consideration (Fig. 4b; see also Fig. 9b, Mitra, 2003). In Fig. 2d, the angle that the line segment $C'Q'$ (correspondingly $C'Q_1'$ and $C'Q_2'$ in Fig. 4) forms with the x axis is the downward deflection angle of the limbs (φ). For the sake of simplicity, the downward deflection angle of both limbs is assumed to be same φ in the following discussion. In each step of folding, there is a corresponding unique value of φ, which maintains the area balanced and the detachment depth constant.

3.1. Constant detachment depth

The principles of the conservation of bed length and cross-sectional area (Hossack, 1979; Homza and Wallace, 1995) are widely recognized. The depth to detachment is determined by the following equation:

$$z = A/(l_0 - l) \tag{5}$$

where z is the theoretical detachment depth; A is the uplifted area in the anticline core (balanced area); l_0 is the arc-length of a reference bed after folding; and l is the fold width (Fig. 4a). This relationship has been widely used since Chamberlin (1910) firstly used it to estimate the detachment depths beneath Appalachian folds. Mitra (2003) improved this method by considering the sinking of rock units in the synclines flanking the anticline. Rock materials are transferred from the synclinal areas to the anticlinal area when a fold initiates. It is required that:

$$A_2' = A_1' - (A_3' + A_4') \tag{6}$$

where A_1' is the excess area above the regional datum; A_2' is the shortened area; A_3' and A_4' are the synclinal areas below the regional datum (Fig. 4b). Taking $S' = l_0 - l'$, the depth to detachment (z) is given by (Mitra, 2003):

$$z = A_2'/S' \tag{7}$$

The constant detachment depth (d) of a natural detachment fold can be calculated from Eq. (5) or other methods (e.g. Bulnes and Poblet, 1999). In the following text, we will introduce a method to find the approximate solution of φ, which makes $z \approx d$ (d is the known constant detachment depth) in each step of folding. The solution is obtained from an approximate equation through an iterative method.

3.2. An approximate equation

In an intermediate step of the early stage of folding, if $\varphi = 0$, $A_1 > A_2$, the area is not balanced (Fig. 4a). Therefore, the application of conventional calculation method leads to an incorrect prediction of the depth to detachment (as $z_0 > d$ in Fig. 4a). Let $S = l_0 - l$:

$$z_0 = A_1/S \tag{8}$$

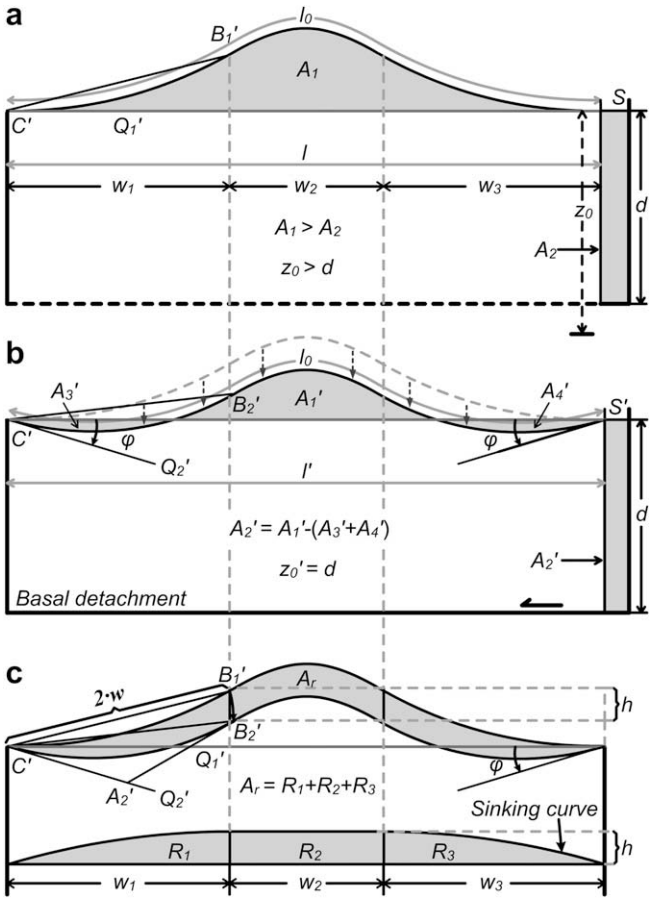

Fig. 4. (a) Fold initials with high wavelength-amplitude ratio will result in an area balancing problem. Since $A_1 > A_2$, application of conventional depth to detachment calculation incorrectly predicts a deep detachment. (b) The downward deflection of the two limbs below the regional datum maintains area balanced. (c) Reduction of balanced area (A_r) is divided into three parts, and can be computed by the integral operation of sinking curve.

where z_0 is the incorrect deep detachment depth. As shown in Fig. 5d, the $z \sim \theta_1$ curve (when $\varphi = 0$) is similar to a hyperbola, which suggests an incorrect deepened detachment depth when the fold initiates and develops.

When $\varphi > 0$ (Fig. 4b), the center part of the fold (including the parts of limb elongation) sinks without deformation, as the limb dips are not changed; in the left and right parts of the fold, the amount of sinking decreases with increasing of horizontal distance to the corresponding inflection points (such as B_1' in Fig. 4a and C'' in Fig. 2d). The upper part of the fold (the gray region in Fig. 4c) represents the deficit area (A_r), which can be expressed as:

$$A_r = (A_1 - A_1') + (A_3' + A_4') \tag{9}$$

Substituting Eq. (6) into this equation gives the following expression for A_r:

$$A_r = A_1 - A_2' \tag{10}$$

On the other hand, A_r can be obtained by integral operation of the sinking curve (Fig. 4c; detail in Appendix A):

$$A_r = w[w_2 + 2/3(w_1 + w_3)]\cdot\varphi \tag{11}$$

where w_1, w_2, w_3 are the horizontal distance between inflection points (points C', B', C'' and B'' in Fig. 2d). This equation implies that area reduction (A_r) is directly proportional to the downward deflection angle (φ).

Let $S' = S$, with Eqs. (7), (8), (10) and (11), and the expression between z and φ is given by:

$$k = -w[w_2 + 2/3(w_1 + w_3)]/(l_0 - l) \tag{12}$$

$$z = z_0 + k\varphi \tag{13}$$

where z_0 is the incorrect deep detachment depth determined by Eq. (8). As w, w_1, w_2, w_3, l and l_0 are known, k is approximate to a constant in a certain intermediate step of folding. Eq. (13) is the approximate equation, which indicates a simple linear relationship between detachment depth (z) and φ. Substitute $z = d$ for Eq. (13), then φ can be expressed as:

$$\varphi = (d - z_0)/k \tag{14}$$

Simulation results from the program are consistent with the relationships from the mathematical derivation. While other parameters are kept constant, a variation of the angle φ produces a series of values for A_r, S and z. The results are plotted on the graphs of Figs. 5a–c, in which φ has been converted into the degree measure. Fig. 5a shows that A_r is directly proportional to φ, which is consistent with Eq. (11). However, as $z = (A_1 - A_r)/S$, the decrease of S (Fig. 5b) results in curvilinear shape of $z \sim \varphi$ (Fig. 5c). Therefore, there is a linear approximate relationship between z and φ, and the linear relationship is more significant when φ increases.

3.3. Iterative method

The iterative operation aims at an approximate solution of φ, which makes z converge to the constant detachment depth (d) in certain intermediate step of folding.

(a) Let $\varphi = \varphi_0 = 0$, A_1 and l_0 can be computed by numerical integration; z_0 is calculated from Eq. (8); and k is computed from Eq. (12).

(b) Let $\varphi = \varphi_1 = (d - z_0) / k$. In this case, A_1', A_3', A_4' and l_0, can also be computed by numerical integration, and detachment depth (z_1) is calculated from Eqs. (6) and (7). The corresponding $z \sim \theta_1$ curve is illustrated in Fig. 5d (when $\varphi = \varphi_1$), which is close to d, yet higher.

(c) Since there is an approximate linear relationship between z and φ, together with the two couples of data (φ_0, z_0) and (φ_1, z_1), φ_2 can be derived as follows:

$$\begin{aligned}(\varphi_2 - \varphi_1)/(\varphi_1 - \varphi_0) &= (d - z_1)/(z_1 - z_0)\\ \varphi_2 &= (d - z_1)\cdot(\varphi_1 - \varphi_0)/(z_1 - z_0) + \varphi_1\end{aligned} \tag{15}$$

Let $\varphi = \varphi_2$, and z_2 can be calculated in a similar way as z_1. The new couples of data (z_2, φ_2), are plotted in Fig. 5d, and the corresponding curve is closer to $z = d$.

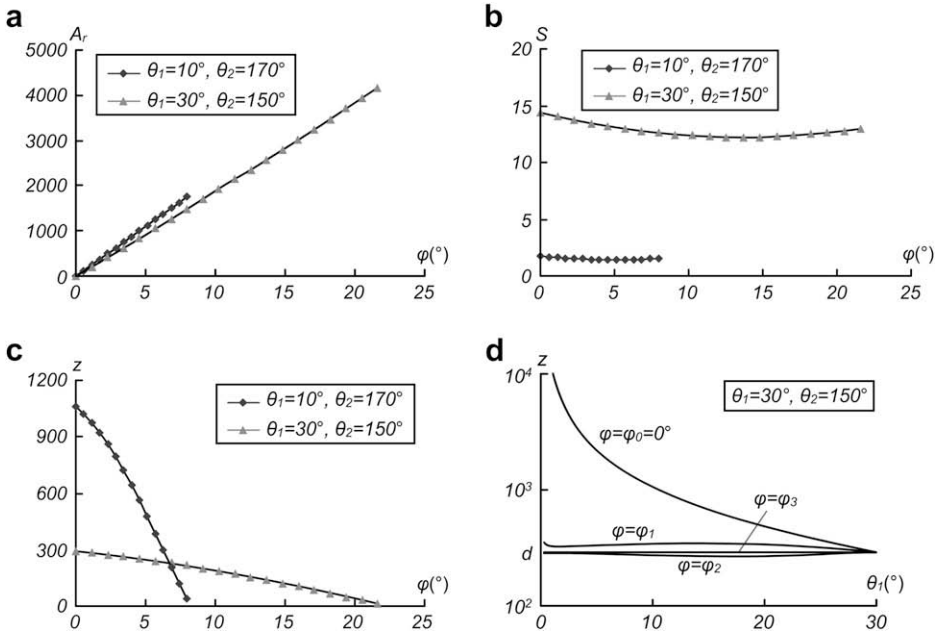

Fig. 5. Simulation results from the program, when $w = 53.33$, $u_c = 0.6$, $u_l = u_r = 0.5$, $E_l = E_r = 0$. (a) The reduction of balanced area (A_r) is directly proportional to the downward deflection angle (φ). (b) However, S is not a constant when φ increases. (c) Since $z = (A_1 - A_r)/S$, the reduction of S will result in curvilinear shape of $z \sim \varphi$. (d) After three times of iterative operation, z converges to the constant detachment depth (d).

(d) As (φ_1, z_1) and (φ_2, z_2) are known, just repeat step (c) until z converges to d.

Simulation results indicate that z approximately converges to d after three iterative operations. In Fig. 5d, when $\varphi = \varphi_3$, the corresponding curve is approximate to a straight line, which suggests the depth to detachment is constant during the folding.

4. Velocity field of syn-folding growth strata

Growth strata offer us the possibility of deciphering kinematic histories of growing structure, which can be divided into pre-growth strata and syn-growth strata. Thinning of units in the hinge zone of anticlines is the main characteristic of syn-folding growth strata. The kinematic histories of growth strata can be deciphered through the process of balanced restoration (Poblet et al., 1997; Casas-Sainz et al., 2005). Here, a new method is used to obtain the velocity field of growth strata of detachment fold, by which the evolution of these strata can also be simulated in the program.

4.1. Velocity field

The pre-growth strata of Figs. 6a–c were illustrated according to the geometric model, and consequently defined by a series of shape parameters. In the kinematic evolution, the fold develops following Eq. 16, and the downward deflection of limbs is not considered ($\varphi = 0$) in order to simplify the description of the method. The velocity field above the pre-growth strata can be obtained by the following numerical calculation method. Firstly, imagine that pseudo strata are stacked on the top of pre-growth strata when a fold initiates. Then, the fold shape is determined by shape parameters in each step of folding. These overlying pseudo layers, which have constant orthogonal thickness, deform entirely by parallel folding. In Figs. 6a–c, seven points have been marked on a pseudo layer to indicate the movement of material, in which point 4 is assumed to be always located on the hinge point. The distances along folded surface between point 4 and other points are constant during the folding to maintain length balance, and consequently the area is kept at a balance, as orthogonal thickness is constant. Therefore, the location of other points can be determined by line integration of curves along the folded surface, which follows constant length principle.

Based on these assumptions, for a certain step of evolution, the velocity of a point can be obtained by subtracting the value of the point coordinates of current step from that of next step. Apply this method to all points on the pseudo layer, the corresponding velocity spectrum is created and shown in Fig. 6d, which indicates that the hinge zone moves upward and two limbs move toward the fold core when the fold initiates. Since the velocity of each point on the overlying growth layers can be obtained by computing the movement of corresponding pseudo layer, the velocity field can be obtained in the program to simulate the movement of growth strata.

4.2. Kink-band migration and limb rotation

Growth strata patterns are controlled by axial plane activity, limb rotation, limb lengthening, fold uplift rates, sedimentation rates and deformation mechanisms of the syn-folding sediments (Poblet et al., 1997). The same fold shape of pre-growth strata can be generated by different mechanisms, such as kink-band migration (variable limb dip and variable limb length) and limb rotation (variable limb dip and constant limb length). However, different mechanisms will result in different shapes of growth strata providing the possibility of deciphering kinematic histories of folds (Suppe et al., 1997; Poblet et al., 1997; Srivastava et al., 1998).

The evolution of growth strata can be simulated by computing velocity field in each step of folding. This syn-folding sedimentation without any erosion has been applied to two deformation mechanisms of the fold: kink-band migration and limb rotation. Simulation result is illustrated in Fig. 7, in which three inflection points I, C'' and B'' (see Fig. 2d) have been marked, indicating the movement of competent rock units. The result shows that the two mechanisms have different final shapes of growth strata, while pre-growth strata are identical. The cross-section of Fig. 7a, which is formed by kink-band migration, shows that "the thickness change in each growth bed is mainly localized in the anticlinal hinge and the fold limb does not vary in dip except in the zone of hinge formation at shallow depths" (Suppe et al., 1997). In contrast, the cross-section of Fig. 7b is formed by limb rotation, recording that "thickness change in each growth bed is spread out over the fold limb, which causes the fold limb to progressively change dip" (see also Fig. 1, Suppe et al., 1997; Figs. 3 and 5, Poblet et al., 1997).

The different growth strata patterns are caused by distinct velocity fields. The velocity vectors of pseudo strata are plotted on Fig. 7, and the length of gray segment indicates the value of velocity. Kink-band migration requires limb lengthening (increase of E)

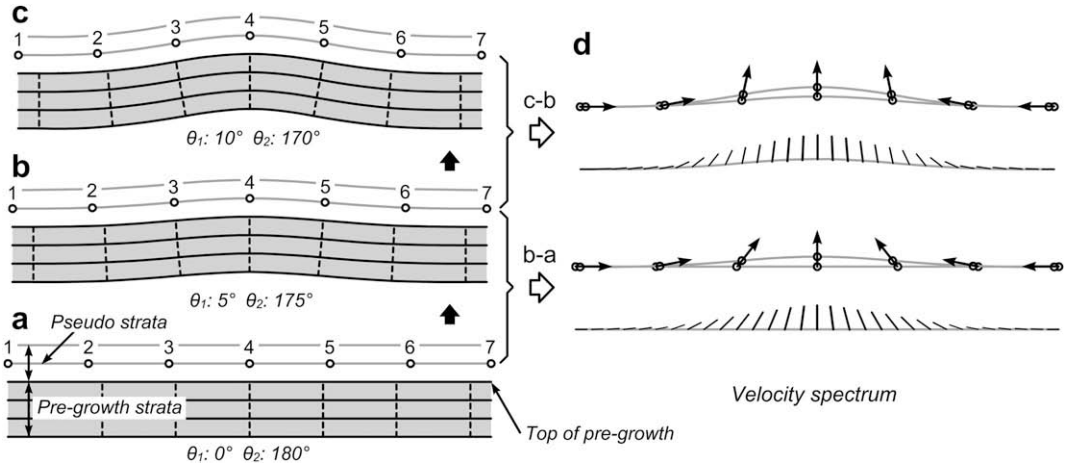

Fig. 6. (a) Pseudo strata are assumed to be stacked on the top of pre-growth strata. Seven points have been marked to indicate the movement of material. (b, c) The pseudo strata develop according to parallel folding model to maintain area and length constant. (d) Velocity spectrum of the pseudo layer can be obtained by computing the displacement of points during the fold evolution.

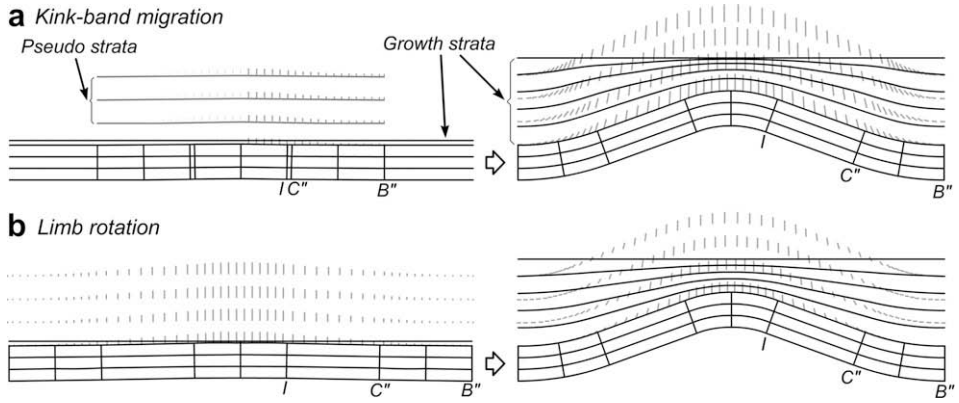

Fig. 7. The growth strata and velocity fields of two mechanisms. (a) Kink-band migration. (b) Limb rotation. In both mechanisms, the sedimentation rate is constant, and the final shape parameters of competent unit are: $\theta_1 = 20$, $\theta_2 = 160$, $E_l = E_r = 2$, $u_l = u_c = u_r = 0.6$. Note: The length of gray segment indicates the value of velocity.

during the folding, while dip angle changes evenly following Eq. (16). Therefore, compared with limb rotation, fold initiates with a lower uplift velocity and end with a greater uplift velocity in this mechanism (compare the gray segment of Fig. 7a with that of Fig. 7b). The fold growth by kink-band migration shows a decreasing thickness of growth strata in the hinge zone (Fig. 7a). Conversely in limb rotation, the axial lift-up rate of the fold is almost unchanged during the folding, which lead to an approximate uniform layer thickness in the hinge.

5. Examples

For illustration of the new model, we apply it to three seismic interpretation maps of detachment folds respectively in Tarim Basin (western China), Zagros fold-belt (Iran) and Niger delta (western Africa). The kinematic numerical simulation of the detachment folds and growth strata were carried out in a program (see the article footnote), developed within the models in this paper.

5.1. A detachment fold, Tarim Basin, Xinjiang Province, China

The cross-section (Fig. 8a) was imported into the program and approximated from the following procedure. Firstly, change the size of the map until the thickness of competent unit matches the default thickness in the program. Secondly, set the limb dips (θ_1 and θ_2) of the default fold according to the natural detachment fold. Thirdly, adjust other parameters (u, E) until the program traces out the given fold shape (Fig. 8b).

In this example, we assume that this fold was formed by limb rotation mechanism, i.e. θ_1 and θ_2 changed evenly, and u and E are constant in the evolution. The initial conditions of the detachment fold are determined by the kinematic assumption: $\theta_{1,0} = 0°$ and $\theta_{2,0} = 180°$. Since the final conditions of the fold have been given, the evolution of the detachment fold can be simulated in the program. The evolution progress is divided into 100 steps. In each step (step n), the fold shape is determined by the shape parameters, which can be calculated from the following equations ($0 \le n \le 100$)

$$\begin{cases} a_{1,n} = a_1 \cdot n/100 \\ a_{2,n} = 180 - (180 - a_2) \cdot n/100 \\ u_n = u; \quad E_n = E \end{cases} \tag{16}$$

In the evolution, downward deflection angle φ_n is computed by the approximate equation and the interactive method.

Fig. 8c illustrates how φ changes during the folding: when $n = 0$, $\varphi = 0$, it corresponds to the initial conditions of the detachment fold; when $n = 100$, $\varphi = 0$, the final fold shape is presented; and when $0 < n < 100$, φ increases at the beginning and return to zero at the end of folding, which indicates the transfer of rock materials between synclinal and anticlinal area. The fold initiates with a high wavelength-amplitude ratio (when n is small), the downward deflection of the two limbs (synclinal areas) maintains area balanced. In the later stages of the folding (when n is close to 100), the units return to their regional positions in the synclines. The simulation result confirms the conclusions of Mitra (2003).

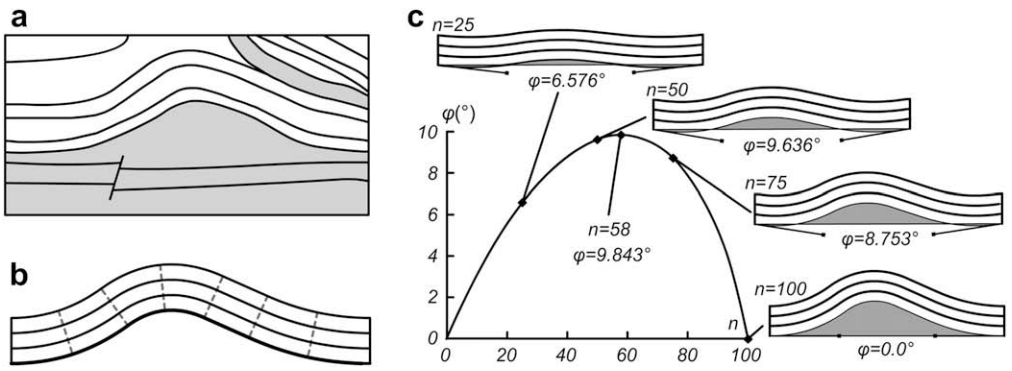

Fig. 8. (a) Seismic interpretation cross-section of a detachment fold, Tarim Basin, Xinjiang Province, China. (b) The competent unit is determined by: $\theta_1 = 36°$, $\theta_2 = 156°$, $u_l = 0.50$, $u_c = 0.52$, $u_r = 0.50$, $E_l = 0$, $E_r = 0.82$ and $\varphi = 0$. (c) The $\varphi \sim n$ curve indicates the transfer of material between synclinal (two limbs) and anticlinal area.

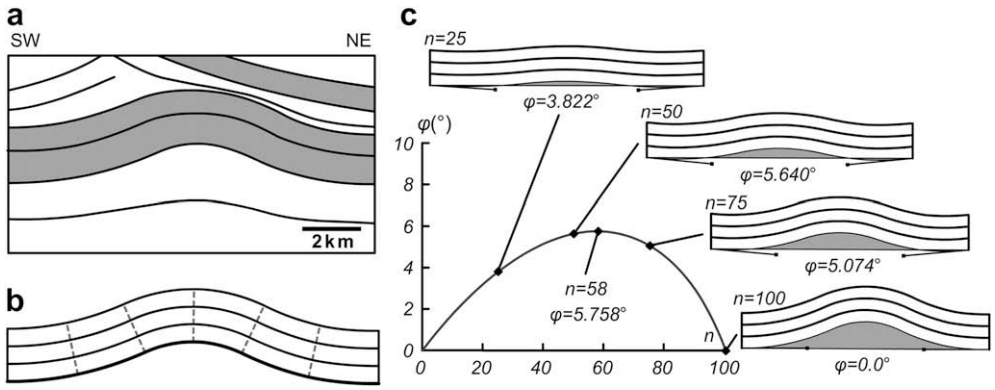

Fig. 9. (a) Seismic interpretation cross-section of a detachment fold, Zagros fold-belt, Iran (modified from Sherkati et al., 2005). (b) The corresponding shape parameters are: $\theta_1 = 24^\circ$, $\theta_2 = 155^\circ$, $u_l = 0.50$, $u_c = 0.50$, $u_r = 0.58$, $E_l = E_r = 0$ and $\varphi = 0$. (c) Compared with the first example, the $\varphi \sim n$ curve of this symmetrical fold shows a smaller φ.

5.2. A detachment fold, Zagros fold-belt, Iran

This seismic interpretation cross-section (Fig. 9a) was approximated following the procedure introduced in the first example. The corresponding shape parameters are: limb dips $\theta_1 = 24^\circ$ and $\theta_2 = 155^\circ$; $E_l = E_r = 0$, which indicate a symmetrical fold shape. We also assume that this fold developed by limb rotation mechanism, and consequently follows Eq. (16).

The simulation result is shown in Fig. 9c, which gives a similar trend of $\varphi \sim n$ curve. This fold also initiates with high wavelength-amplitude ratio, and deflection angle increases at the beginning and returns to zero at the end of folding. However, compared with the first example, limb dips and limb elongation are smaller in this detachment fold, i.e., a smaller excess area. According to Eq. (11), φ is directly proportional to A_r. As a result, the maximum deflection angle is smaller in this detachment fold.

5.3. A detachment fold with growth strata, Niger delta, western Africa

This detachment fold with growth strata (Fig. 10a) lies at 1.5 km water depth within the passive-margin fold-and-thrust belt of the Niger delta, offshore Nigeria (Bilotti and Shaw, 2005; Gonzalez-Mieres and Suppe, 2006). A strong about 4° landward dipping reflector at 10–11 km depth results in the west limb of this otherwise symmetric anticline to have lower dip compared with that of the east limb.

The core of the fold shows a substantial excess area, which may involve far-field injection of mobile material (Gonzalez-Mieres and Suppe, 2006). Therefore, downward deflection of limbs is not considered in the simulation, i.e. $\varphi \equiv 0$ in the folding. In Fig. 10a, the shape of growth strata is similar to that of Fig. 7b, which is formed by limb rotation mechanism. As a result, in kinematic simulation, the fold develops step by step following Eq. (16); velocity field was created by computing the movement of pseudo strata; and finally, the kinematic simulation of the fold and growth strata can be carried out in the program. The interpreted cross-section (Fig. 10a) and the simulation map (Fig. 10b) are in good agreement, which suggests mainly limb rotation mechanism (Bilotti and Shaw, 2005).

6. Discussions and conclusions

The model of detachment folds and growth strata is based on quadratic Bézier curves, and involves joining together several segments of the Bézier curves to approximate fold shape. The basic three parameters, w, θ_1 and θ_2, define an ideal detachment fold. In order to simulate complex natural folds, two more parameters u and E are used to control the axial lift-up ratio and the limb elongation respectively.

In the kinematic modeling of detachment folds, area balancing requires downward deflection of synclines flanking anticline. An approximate equation and an interactive method are developed to compute the approximate solution of downward deflection angle (φ), which maintains the area balanced and detachment depth constant in the kinematic evolution. In the process of derivation, a new area parameter, A_r represents the reduction of the balanced area when downward deflection of two limbs is considered. Both mathematical derivation and simulation results show a direct proportional relationship between A_r and φ, and a linear approximate relationship between detachment depth (z) and φ. In the examples, the $\varphi \sim n$ curve indicates the transfer of material between synclinal and anticlinal area during the folding, which is confirmed by previous studies.

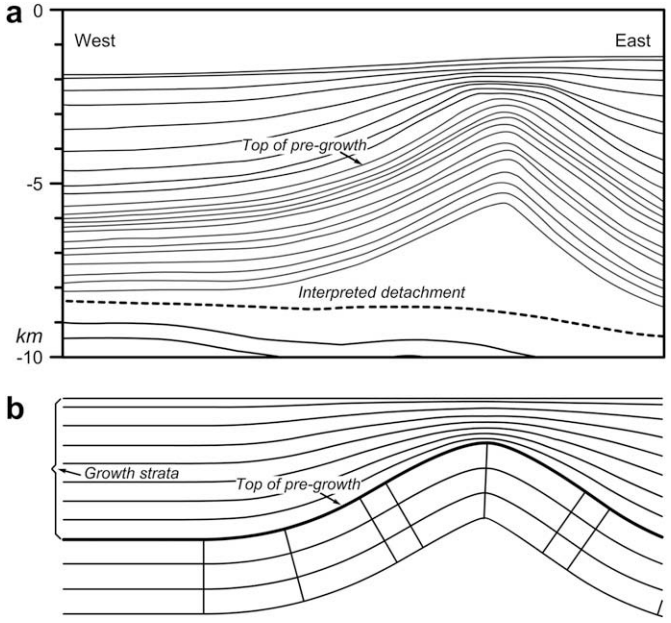

Fig. 10. (a) Seismic interpretation cross-section of a detachment fold and growth strata, Niger delta, western Africa (modified from Gonzalez-Mieres and Suppe, 2006; the right part of this cross-section, which involved in secondary folding, has been cut out). (b) The simulation cross-section that formed by limb rotation is determined by these parameters: $\theta_1 = 30^\circ$, $\theta_2 = 145^\circ$, $u_l = 0.50$, $u_c = 0.85$, $u_r = 0.50$, $E_l = E_r = 0.3$.

Further, this paper has introduced a method to create velocity field by computing the movement of pseudo strata. In order to show the feasibility of simulating the evolution of growth strata and deciphering kinematic histories of folds, this method is applied to a detachment fold to simulate its evolution with growth strata. The disadvantage of the method is that it is only applicable to the folds with gentle dips and approximate uniform curvature distribution between hinge points and inflection points, since steep dips or concentrated curvature distribution will lead to an impossible cuspate shape in the limbs of pseudo layers. However, this method still provides a good result when the limb dip is less than 30° and the axial lift-up ratio (u_l and u_r) is between 0.4 and 0.6. Note that the folded surface shows an approximate uniform curvature distribution in Fig. 3, when u is 0.5.

We have assumed that the folds develop evenly, and shape parameters are changed regularly in the kinematic evolution. Actually, a fold may remain one limb dip unchanged while the other dip increases. More research should focus on the hinge migration and the limb rotation in this model, and more functions should be added to this model in order to deal with these new situations. Furthermore, the numerical simulation method of growth strata needs to be improved, since the present method is confined to the folds with gentle dips. These may be regarded as the next objective of research.

Acknowledgements

Financial support from Natural Science Foundation of China (NSFC, NO. 40572119 granted to Dr. Yikun Zhang) is appreciated. The idea of using Bézier curves to simulate folds arose out of discussions with Professor Zhu Guorong. We are grateful to JSG reviewers, Professors Bastida and Srivastava, for many valuable suggestions that have notably helped us to improve the manuscript.

Appendix A: Computation of A_r (reduction of balanced area)

We will describe here how to obtain A_r, i.e., Eq. (11). Fig. 11a is modified from the top left corner of Fig. 4c, which indicates the movement of points and lines when downward deflection of limbs is considered. The length, h, which represents the sinking of center part (Fig. 4c), is approximate to the length of arc $B_1'B_2'$, which can be derived following.

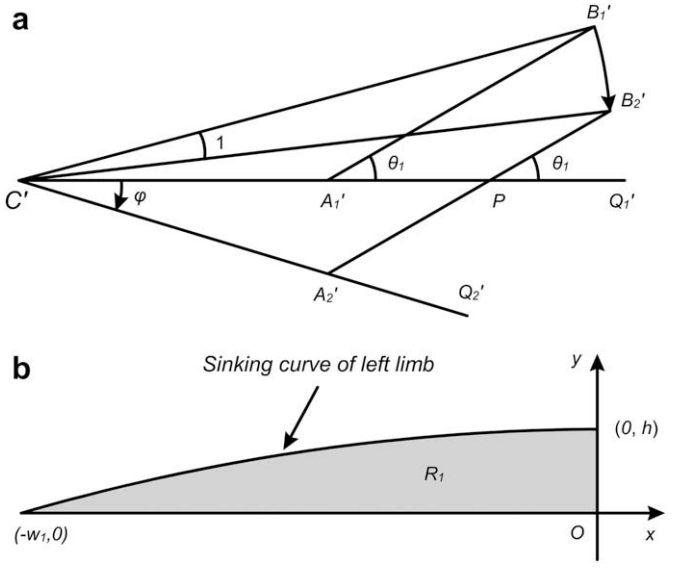

Fig. 11. (a) When the limb sinks into bed, points B', A' and Q' (in Fig. 2d) are moved to the position of points B_2', A_2' and Q_2', respectively. (b) R_1 (see Fig. 4c) can be obtained by integral operation of the parabola.

$A_1'B_1'C'$ is an isosceles triangle (see also triangle $A'B'C'$ in Fig. 2d), therefore:

$$\angle B_1'C'Q_1' = \angle B_1'A_1'Q_1'/2 = \theta_1/2 \tag{A1}$$

where θ_1 is the dip angle of left limb. When the limb sinks into bed, points B', A' and Q' (in Fig. 2d) are moved to the position of points B_2', A_2' and Q_2', respectively; the angles that $C'Q_2'$ and $B_2'A_2'$ form with the horizontal axis ($C'Q_1'$) are φ and θ_1, respectively. $A_2'B_2'C'$ is also an isosceles triangle, therefore:

$$\angle B_2'C'Q_2' = \angle B_2'A_2'Q_2'/2 \tag{A2}$$

with

$$\begin{aligned}\angle B_2'A_2'Q_2' &= \angle C'PA_2' + \angle Q_1'C'Q_2' \\ &= \theta_1 + \varphi\end{aligned}$$

Eq. (A2) is expressed as:

$$\angle B_2'C'Q_2' = (\theta_1 + \varphi)/2 \tag{A3}$$

and consequently

$$\begin{aligned}\angle B_2'C'Q_1' &= \angle B_2'C'Q_2' - \varphi \\ &= (\theta_1 - \varphi)/2\end{aligned} \tag{A4}$$

with Eqs. (A1) and (A4), $\angle 1$ can be calculated from:

$$\angle 1 = \angle B_1'C'Q_1' - \angle B_2'C'Q_1' = \varphi/2 \tag{A5}$$

The length of segment $B_1'C'$ is known:

$$l_{B_1'C'} = 2w \tag{A6}$$

therefore, the approximate solution of sinking is given by:

$$\text{Arc } B_1'B_2' = l_{B_1'C'} \cdot \angle 1 = (2w)\cdot(\varphi/2) = w\varphi$$

$$h \approx \text{Arc } B_1'B_2' = w\varphi \tag{A7}$$

The lower part of Fig. 4c shows that A_r can be calculated by the integral operation of the sinking curve, which is divided into three parts: R_1, R_2 and R_3. The center part of sinking curve is a horizontal segment, therefore, R_2 is calculated from:

$$R_2 = w_2 h \tag{A8}$$

The corresponding sinking curve segments of two limbs are close to parabolas (Fig. 4c). Therefore, the gray region under the curve segments can be calculated by integral operation of the parabolas. The sinking curve of the left limb is redrawn on the coordinates of Fig. 11b. Since the highest point of the parabola is located on the y axis, the definition equation of this curve can be written as:

$$f(x) = ax^2 + b$$

where a and b are unknown coefficients. Substitute $(0, h)$ and $(-w_1, 0)$ into this equation, the two coefficients are obtained. Then, the definition equation is given by:

$$f(x) = -\frac{h}{w_1^2}\cdot x^2 + h \tag{A9}$$

therefore, R_1 can be calculated from:

$$R_1 = \int_{-w_1}^{0} f(x) = 2/3 w_1 h \tag{A10}$$

Similarly

$$R_3 = 2/3 w_3 h \quad \text{(A11)}$$

with Eqs. (A8), (A10) and (A11), A_r is obtained:

$$A_r = R_1 + R_2 + R_3 = w[w_2 + 2/3(w_1 + w_3)]\cdot\varphi \quad \text{(A12)}$$

Appendix B: Abbreviations

θ_1 dip angle of left limb
θ_2 dip angle of right limb
w the parameter used to describe the size of a fold
α dip angle of axial plane
β $\beta = (\theta_2 - \theta_1)/2$
u axial lift-up ratio
E limb elongation
φ downward deflection angle of limbs
z theoretical detachment depth
z_0 incorrect deep detachment depth
d constant detachment depth
l_0 Arc-length of a reference bed after folding
l fold width
S shortening
S' shortening (deflection of limbs)
h sinking of center part, i.e. max sinking
A_1 excess area above regional datum
A_2 shortened area
A_1' excess area above regional datum (deflection of limbs)
A_2' shortened area (deflection of limbs)
A_3' A_4' synclinal areas below the regional position
A balanced area
A_r reduction of balanced area (A) when downward deflection of limbs is considered

References

Bastida, F., Aller, J., Bobillo-Ares, N.C., 1999. Geometrical analysis of folded surfaces using simple functions. Journal of Structural Geology 21, 729–742.

Bézier, P., 1966. Definition numérique des corbes et surfaces-I. Automatisme 11, 625–632.

Bézier, P., 1967. Definition numérique des corbes et surfaces-II. Automatisme 12, 17–21.

Bilotti, F., Shaw, J., 2005. Deep-water Niger Delta fold and thrust belt modeled as a critical-taper wedge: the influence of elevated basal fluid pressure on structural styles. American Association of Petroleum Geologists Bulletin 89, 1475–1491.

Biot, M.A., 1961. Theory of folding of stratified viscoelastic media and its implications in tectonics and orogenesis. Geological Society of America Bulletin 72, 1595–1620.

Bulnes, M., Poblet, J., 1999. Estimating the detachment depth in cross sections involving detachment folds. Geological Magazine 136, 395–412.

Casas-Sainz, A.M., Soto-Marin, R., Gonzaleza, A., Villalain, J.J., 2005. Folded onlap geometries: implications for recognition of syn-sedimentary folds. Journal of Structural Geology 27, 1644–1657.

Chamberlin, R.T., 1910. The Appalachian folds of central Pennsylvania. Journal of Geology 18, 228–251.

Chapple, W.M., 1969. Fold shape and rheology; the folding of an isolated viscous-plastic layer. Tectonophysics 7, 97–116.

Coelho, S., Passchier, C., Grasemann, B., 2005. Geometric description of flanking structures. Journal of Structural Geology 27, 597–606.

Currie, J.B., Patnode, H.W., Trump, R.P., 1962. Developments of folds in sedimentary strata. Geological Society of America Bulletin 73, 655–674.

De Paor, D.G., 1996. Bèzier curves and geological design. In: De Paor, D.G. (Ed.), Structural Geology and Personal Computers. Pergamon Press, pp. 389–417.

Gonzalez-Mieres, R., Suppe, J., 2006. Relief and shortening in detachment folds. Journal of Structural Geology 28, 1785–1807.

Homza, T.X., Wallace, W.K., 1995. Geometric and kinematic models for detachment folds with fixed and variable detachment depths. Journal of Structural Geology 17, 575–588.

Hossack, J.R., 1979. The use of balanced cross-sections in the calculation of orogenic contraction: a review. Journal of the Geological Society of London 136, 705–711.

Hudleston, P.J., 1973. Fold morphology and some geometrical implications of theories of fold development. Tectonophysics 16, 1–46.

Mitra, S., 2003. A unified kinematic model for the evolution of detachment folds. Journal of Structural Geology 25, 1659–1673.

Poblet, J., McClay, K., Storti, F., Munoz, J.A., 1997. Geometries of syntectonic sediments associated with single-layer detachment folds. Journal of Structural Geology 19, 369–381.

Scharer, K.M., Burbank, D.W., Chen, J., Weldon, R.J., Rubin, C., Zhao, R., Shen, J., 2004. Detachment folding in the Southwestern Tian Shan-Tarim foreland, China: shortening estimates and rates. Journal of Structural Geology 26, 2119–2137.

Sherkati, S., Molinaroc, M., Frizon de Lamotte, D., Letouzey, J., 2005. Detachment folding in the Central and Eastern Zagros fold-belt (Iran): salt mobility, multiple detachments and late basement control. Journal of Structural Geology 27, 1680–1696.

Srivastava, D.C., Lisle, R.J., 2004. Rapid analysis fold shapes using Bézier curves. Journal of Structural Geology 26, 1553–1559.

Srivastava, D.C., Lisle, R.J., Imran, M., Kandpal, R., 1998. The kink-band triangle: a triangular plot for paleostress analysis from kink-bands. Journal of Structural Geology 20, 1579–1586.

Stabler, C.L., 1968. Simplified Fourier analysis of fold shapes. Tectonophysics 6, 343–350.

Sun, J.G., Hu, S.D., 2005. Computer graphics tutorial. Tsinghua University Press, Beijing, pp. 27-30.

Suppe, J., Sábat, F., Munoz, J.A., Poblet, J., Roca, E., Vergés, J., 1997. Bed-by-bed fold growth by kink-band migration: Sant llorenç de Morunys, eastern Pyrenees. Journal of Structural Geology 19, 443–461.

Twiss, R.J., 1988. Description and classification of folds in single surfaces. Journal of Structural Geology 10, 607–623.

Wilkerson, M.S., Smaltz, S.M., Bowman, D.R., et al., 2007. 2-D and 3-D modeling of detachment folds with hinterland inflation: a natural example from the Monterrey Salient, northeastern Mexico. Journal of Structural Geology 29, 73–85.